Broadband Spectral Induced Polarization for the detection of Permafrost and an approach to ice content estimation – A Case study from Yakutia, Russia

Jan Mudler[1], Andreas Hördt[1], Dennis Kreith[1], Kirill Bazhin[2], Lyudmila Lebedeva[2], and Tino Radić[3]

[1]Technische Universität Braunschweig, Institut für Geophysik und extraterrestrische Physik, Braunschweig, Germany
[2]Melnikov Permafrost Institute, Russian Academy of Science, Yakutsk, Russia
[3]Radic Research, Berlin, Germany

Correspondence: Jan Mudler (j.mudler@tu-bs.de)

Abstract. The reliable detection of subsurface ice using non-destructive geophysical methods is an important objective in permafrost research. Furthermore, the ice content of the frozen ground is an essential parameter for further interpretation, for example in terms of risk analysis, e.g. for the description of permafrost carbon feedback by thawing processes.

The High-Frequency Induced Polarization method (HFIP) enables the measurement of the frequency dependent electrical sig-

5   nal of the subsurface. In contrast to the well-established Electrical Resistivity Tomography (ERT), the usage of the full spectral information provides additional physical parameters of the ground. As the electrical properties of ice exhibit a strong characteristic behaviour in the frequency range between $100\,\mathrm{Hz}$ and $100\,\mathrm{kHz}$, HFIP is in principle suitable to estimate ice content. Here, we present methodological advancements of the HFIP method and suggest an explicit procedure for ice content estimation.

A new measuring device, the Chameleon-II (Radic Research), was used for the first time. It was designed for the application of

10 Spectral Induced Polarization over a wide frequency range and is usable under challenging conditions, for example in field sites under periglacial influence and the presence of permafrost. Amongst other improvements, compared to a previous generation, the new system is equipped with longer cables and larger power, such that we can now achieve larger penetration depths up to $10\,\mathrm{m}$. Moreover, it is equipped with technology to reduce electromagnetic coupling effects which can distort the desired subsurface signal.

15 The second development is a method to estimate ice content quantitatively from five Cole-Cole parameters obtained from spectral two-dimensional inversion results. The method is based on a description of the subsurface as a mixture of two components (matrix and ice) and uses a previously suggested relationship between frequency-dependent electrical permittivity and ice content.

Measurements on a permafrost site near Yakutsk, Russia, were carried out to test the entire procedure under real conditions at

20 the field scale. We demonstrate that the spectral signal of ice can clearly be identified even in the raw data, and show that the spectral 2-D inversion algorithm is suitable to obtain the multidimensional distribution of electrical parameters. The parameter distribution and the estimated ice content agree reasonably well with previous knowledge of the field site from borehole and geophysical investigations. We conclude that the method is able to provide quantitative ice content estimates, and that relationships that have been tested in the laboratory may be applied at the field scale.

1 Introduction

The frequency dependent electrical properties of ice have been studied by several authors over the past decades in the laboratory for pure ice as well as for ice within sediment mixtures (e.g. Auty and Cole, 1952; Hippel, 1988; Bittelli et al., 2004; Grimm et al., 2015; Artemov, 2019). A limited number of field studies has been reported as well (e.g. Grimm and Stillman, 2015; Przyklenk et al., 2016). The permittivity of water ice exhibits a characteristic frequency-dependence in the frequency range between $100\,\mathrm{Hz}$ and $100\,\mathrm{kHz}$ (Petrenko and Whitworth, 2002; Artemov and Volkov, 2014). At the field scale, ice often does not occur in its pure form within the subsurface, but in mixtures with sediments, as in frozen ground. The ice content of permafrost is an important piece of information, e.g. for risk analysis for humans and infrastructure (Hauck and Kneisel, 2008; Heginbottom et al., 2012) and for the description of the permafrost carbon feedback by thawing process due to climate change (Schuur et al., 2015).

In geophysics, models for the estimation of ice content use the contrast of characteristic physical material properties to distinguish ice from the other components of the subsoil. Since the pure data of electrical resistivity tomography (ERT) does not provide enough information for a quantitative ice content estimation, Hauck et al. (2011) use a combination of ERT and seismic measurements to separate the subsoil into four components: the soil matrix (i.e. rock), ice, water and air. A joint 2-D inversion based on this model was presented by Wagner et al. (2019) and successfully applied to several alpine field sites by Mollaret et al. (2020).

Attempts have been made to estimate ice content with one method only. A promising parameter is the frequency-dependent electrical permittivity. Therefore, models of four and three components have been suggested by Bittelli et al. (2004) and Stillman and Grimm (2010). Theoretical investigations about the frequency-dependent electrical behaviour of frozen ground due to the polarization processes of ice were carried out by Kozhevnikov and Antonov (2012) and Zorin and Ageev (2017), with the aim to relate ice content directly to electrical permittivity. They assume fully saturated and frozen conditions, in which case the number of phases reduces to two (ice and matrix). An empirical approach was suggested by Grimm and Stillman (2015) who did not use the full spectral information but calculated the difference between electrical resistivity at two discrete frequencies. The calibration of the difference to estimate ice content is then based on laboratory investigations.

While the relationship between ice content and electrical permittivity has been well studied in the laboratory and with theoretical investigations, there is almost no experience at the field scale. A common geophysical method for the acquisition of the frequency dependent electrical signal of the subsurface is the Spectral Induced Polarization (SIP). While conventional SIP is typically used in the frequency range $< 1\,\mathrm{kHz}$ (Kemna et al., 2000), the measurement of the full process of ice relaxation requires the usage of high-frequency IP (HFIP) with enlarged frequency range up to $100\,\mathrm{kHz}$. The first application of broadband detection of electrical parameters at the field scale was reported by Grimm and Stillman (2015). Przyklenk et al. (2016) obtained field data over pure ice with a system specifically designed for broadband data acquisition in combination with capacitive coupling. They discussed different parameterizations of frequency-dependent permittivity and the possibilities to resolve the parameters based on a homogeneous halfspace assumption. Mudler et al. (2019) discussed several case histories in different regions and suggested an approach at a two-dimensional inversion. Limbrock and Weigand (2020) obtained broad-band data

from alpine permafrost sites by field measurements and from laboratory investigations. They investigated the spectral signal in terms of thermal ground characteristics.

The previous studies were limited to qualitative interpretation with respect to ice content. Partly due to the lack of penetration depth of the acquisition system, the assumption of a homogeneous halfspace was usually sufficient, or a real situation where

5 variable ice content existed was not met. Here, we present the next logical steps towards a system that can help to estimate ice content in practical situations. We further advanced the acquisition system; one of the aims being a larger penetration depth. The 'Chameleon II' is a system for the broad-band spectral detection of complex electrical signal and for the usage under challenging field conditions. We also developed a method to estimate ice content from the electrical parameters that can actually be determined by the 2-D inversion approach.

10 To demonstrate the feasibility of the method, we carried out a field survey at the Shestakovka River Basin, near the Russian City Yakutsk. Investigations by Lebedeva et al. (2019) confirmed the presence of permafrost within the first few meters of depth and the occurrence of an unfrozen water-bearing talik within the frozen ground. The results will be compared with existing knowledge of the subsurface from a borehole and geophysical investigations.

2 Electrical permittivity of frozen soil

15 The complex electrical impedance of the ground is measured in terms of its magnitude $|Z|$ and phase shift $\varphi(Z)$ over a wide frequency range at several discrete frequencies. It contains the full information about the two material dependent properties of the ground: the electrical resistivity ρ and the relative dielectric permittivity ε_r. The two properties are responsible for the behaviour of dissipation and storage of electromagnetic energy, and these mechanisms may be expressed in combination by the complex relative permittivity ε_r^* as follows:

$$\varepsilon_r^*(\rho, \varepsilon_r, \omega) = \varepsilon_r' - i\varepsilon_r'' = \varepsilon_r + \frac{1}{i\omega\varepsilon_0\rho}, \qquad (1)$$

where ε_r' and ε_r'' are the real and imaginary part of the complex relative dielectric permittivity, with the permittivity of free space $\varepsilon_0 = 8.854 \times 10^{-12} F\ m^{-1}$, the angular frequency ω and the imaginary unit $i = \sqrt{-1}$.

25 Many natural materials and material compositions show a frequency dependent behavior in electrical properties, due to polarization effects. Several reasons for polarizability are known, which can be distinguished by their strength and their occurrence in frequency range (Loewer et al., 2017). A mathematical description of those effects can be achieved by a parametrization of the frequency dependent permittivity. As discussed by Mudler et al. (2019), a useful parameterization for 2-D inversion is the model suggested by Cole and Cole (1941) in terms of the effective complex relative permittivity, of the form:

30

$$\varepsilon_r^* = \varepsilon_{HF} + \frac{\varepsilon_{DC} - \varepsilon_{HF}}{1 + (i\omega\tau)^c} + \frac{1}{i\omega\varepsilon_0\rho_{DC}}. \qquad (2)$$

The five Cole-Cole parameters are: the direct current (DC) resistivity ρ_{DC}, the low-frequency limit ε_{DC} and the high-frequency limit ε_{HF} for the permittivity, the relaxation time τ and the relaxation exponent c. The equation represents the behaviour for low frequencies dominated by the resistivity, the behaviour for high frequencies controlled by the permittivity, and the part of relaxation process occurring in between (Grimm and Stillman, 2015). In the case of pure ice, the relaxation process can be approximated by the Debye model, which is a special case of a Cole-Cole model with fixed exponent $c = 1$, resulting in a reduction of free model parameter to four (e.g. Petrenko and Whitworth, 2002; Artemov and Volkov, 2014).

The strong relaxation process of ice occurs around a relaxation time τ of $2 \times 10^{-5}\,\mathrm{s}$ at $0°C$, shifting to longer times for decreasing temperature (Sasaki et al., 2016). Therefore, the detection of the ice relaxation requires frequency measurements in the range of kHz. Our system was designed to measure in a range up to above $100\,\mathrm{kHz}$. In areas under periglacial conditions, due to high values of permittivity and resistivity of ice (Hauck and Kneisel, 2008), both mechanisms, the conduction and displacement currents, influence the signal of the impedance within the measured frequency range.

3 Ice content estimation

The HFIP method uses the same field procedures as DC resistivity methods. In principle, soundings and tomographic measurements in different configurations, such as Wenner and Schlumberger, are available, but the dipole-dipole configuration is generally preferred because it is less sensitive to EM coupling effects.

The measured impedance spectra can be analyzed either separately, or in a two-dimensional inversion algorithm. Both procedures are described by Mudler et al. (2019) and use the Cole-Cole model (eq. 2) to fit the spectral data. The first approach can be used to evaluate single spectra to give an overview of the subsurface information or in case of homogeneous grounds or samples, as in laboratory studies. To obtain the spatial distribution of electrical parameters, a 2-D inversion algorithm embedded in the geophysical modelling and inversion toolbox AarhusInv (Auken et al., 2014) was developed and presented by Mudler et al. (2019). The inversion leads to the distribution of all five model parameters, which can be visualized in separate two-dimensional sections. Therefore, an interpretation of subsurface material and structure based on the full spectral information is possible.

Here, we add another step to the data analysis - the quantitative estimation of ice content. Several models for ice content estimation based on the frequency dependent electrical information of subsurface material exist in the literature, based on empirical approaches (e.g. Bittelli et al., 2004; Stillman and Grimm, 2010) and on physical models, such as the Maxwell-Wagner polarization, (e.g. Kozhevnikov and Antonov, 2012; Zorin and Ageev, 2017). The models have been developed theoretically and have been tested with laboratory data of frozen samples. Under laboratory conditions, additional measurements, such as the saturation of the sample or the permittivity of the unsaturated matrix material can be performed. However, none of the existing theories or empirical relationships estimates the ice content using the five parameters we can actually obtain from field measurements. Therefore, we suggest an additional inversion that is applied to the results of the spatial 2-D inversion and converts the five parameters into ice content. Our method is based on the theory of Zorin and Ageev (2017), which describes

the subsurface material as a two-component mixture of ice and an ice-free part of the soil. In that theory it is assumed, that the polarization is fully caused by the ice fraction. The complex electrical conductivity represents a power mean of both components weighted by the ice content α:

$$\tilde{\sigma}_b^k(\omega) = (1 - \alpha)\,\tilde{\sigma}_m^k(\omega) + \alpha\,\tilde{\sigma}_i^k(\omega) \tag{3}$$

where $\tilde{\sigma}$ are the complex conductivities ($\tilde{\sigma} = i\omega\varepsilon^*$) of the bulk soil (b), the ice (i) and the ice-free matrix material (m). As the ice-free part is assumed to be non-polarizing, its complex conductivity can be described by constant electrical parameters over frequency:

$$\tilde{\sigma}_m(\omega) = \sigma_m + i\omega\varepsilon_0\varepsilon_m \tag{4}$$

with σ_m and ε_m being the DC conductivity and the relative permittivity of the ice-free matrix. The matrix itself may be a composition of different materials, which are considered to be included in the electrical parameters, which constitutes an effective matrix conductivity. The possible presence of water is included in this fraction as well, because the electrical parameters of water are constant in the examined frequency range. The polarization processes for water takes place at higher frequencies ($> 1\,\mathrm{GHz}$) (Artemov, 2019).

The frequency dependent behaviour of the ice signal can be described by a Debye model, formally equivalent to (eq. 2), written down for conductivity with $c = 1$:

$$\tilde{\sigma}_i(\omega) = \sigma_{i,DC} + i\omega\varepsilon_0\left(\varepsilon_{i,HF} + \frac{\varepsilon_{i,DC} - \varepsilon_{i,HF}}{1 + i\omega\tau_i}\right) \tag{5}$$

with $\sigma_{i,DC}$ being the DC conductivity of ice, $\varepsilon_{i,HF}$ and $\varepsilon_{i,DC}$ the low and high frequency limit of the relative permittivity of ice and τ_E the relaxation time for ice. The exponent k in eq. 3 is assumed to reflect the spatial microstructure of both components, with $k \in [-1, 1]$. For a detailed discussion of the different values for k see Zorin and Ageev (2017). Overall, eq. 3 comprises eight free parameters: the ice content α, the formation exponent k, the two electric parameters of the ice-free part and the four electric parameters of the ice part. Fortunately, the three electrical parameters describing the relaxation of pure ice, are well known and can be fixed, namely the high and low frequency permittivity $\varepsilon_{i,HF}$ and $\varepsilon_{i,DC}$ and the relaxation time τ_i. This reduces the number of unknowns to five, which is equal to the number of parameters that we obtain from the field measurements. We can therefore proceed to obtain the five unknowns of the two-component model, ice content being one of them.

To estimate ice content of a homogeneous sample, e.g. in the laboratory, measured spectra can be directly fitted to eq. 3. In the

case of heterogeneous field data, the distribution of electrical parameters within the subsurface, has to be determined first. In our application, we use the inverted 2-D spectra as input for the fitting process and thus get the two-dimensional distribution of ice content. The algorithm is implemented in MATLAB 2017b using the nonlinear least square solver (lsqnonlin).

4   Chameleon II Instrument

5   Impedance measurements at the field scale with 4-point configurations up to $230\,\mathrm{kHz}$ place special demands on the hardware . Unlike quasi DC measurements, capacitive and inductive coupling effects occur at high frequencies, which, if not taken into account, lead to irreversibly disturbed measurement results. Most of the coupling occurs between the measuring cables themselves and between them and the ground. In principle, inductive coupling can be calculated with suitable simulation programs. In addition to the position of the current and potential electrodes, the known course of the measuring cables must be taken
10   into account. The situation is different with capacitive coupling effects. Here, quantitative modelling is complicated by the fact that the strength of the coupling is determined, among other things, by the coupling resistances of the two current electrodes, as well as the distance of the current cables from the ground. Both are usually not known with sufficient accuracy. Capacitive coupling must therefore a priori be avoided as far as possible during the measurement with the help of a suitable measurement concept.
15   We drew on experience with a prototype "Chameleon-I" (Radić, 2013) which we optimized in several ways. Field measurements showed (Przyklenk et al., 2016) that the measurement concept used is at least suitable for small-scale investigations of highly resistive ground. However, most permafrost sites and in particular the site in Yakutia discussed further below, require the exploration of greater depths. For this purpose, the Chameleon-I concept had to be further advanced. Larger measurement configurations require a more powerful transmitter and additional measures to reduce the stronger coupling effects associated
20   with longer measurement lines. Figure 1 shows the block diagram of the Chameleon-II instrument. An essential innovation is that a complete transmitter is now positioned at each of the two current electrodes. In contrast to the previous instrument, this results in a symmetrical current dipole. Both transmitters are connected in series via a power cable. As a result, the two transmitter voltages add up to ±800 volts. Thanks to the symmetry of the current dipole, there is no more need for lossy shielding of the current cable as with the Chameleon-I. In practice, the current electrodes have unequal contact resistances. The result is a
25   more or less large potential difference between the current cable connecting the two transmitters and the ground below. At the high measurement frequencies used, this causes considerable capacitive leakage currents, which inevitably lead to systematic measurement errors. The presence of leakage currents can be reliably detected by comparing the current strengths measured in the transmitters, directly at the current electrodes. The larger the leakage current or the potential difference, the stronger the measured current strength difference. The output voltage of the two transmitters can be set individually. If one changes their
30   amplitude ratio, the potential difference between the power cable and the ground changes and consequently also the difference of the two current strengths. With a suitable choice of the voltage amplitude ratio, the potential difference disappears, the two current strengths equalize and a measurement error caused by leakage current is minimized. Undesirable potential differences also occur to a lesser extent between the potential cables and the ground below. To minimize the negative effects on the voltage

measurement, active probes are used directly at the potential electrodes.

In addition to the EM distortion resulting from the direct coupling of the cables with each other and to the ground, there is also the effect of induced currents in the ground, which can not be avoided. Mudler et al. (2019) suggested equations based on the theory developed by Weidelt (1997) to estimate whether induction effects can be ignored. Induction effects are particularly

5   strong in case of high frequencies, large spatial scales and low resistivities. Compared to previous measurements of the HFIP method (Przyklenk et al., 2016; Mudler et al., 2019), we are using larger spacings, and therefore, an individual evaluation is required. Assuming subsurface resistivities higher than $2000\,\Omega\mathrm{m}$ for the top layer, according to fig. 3 and Lebedeva et al. (2019), induction effects are small enough to be neglected over almost the entire measuring range. For the highest frequencies and largest configurations, the conditions for neglecting induction are no longer strictly fulfilled and might have to be considered

10   explicitly by modelling in future work.

Both instruments (Chameleon-I and Chameleon-II) can be used with capacitive electrodes, namely the Capacitively Coupled Resistivity method (CCR), applied by Przyklenk et al. (2016) and Mudler et al. (2019). Impedance measurements using conventional galvanic electrode coupling can be applied as well. As the logistical advantages of capacitive coupling were not significant at our field site in Yakutia, measurements were conducted using galvanic coupling.
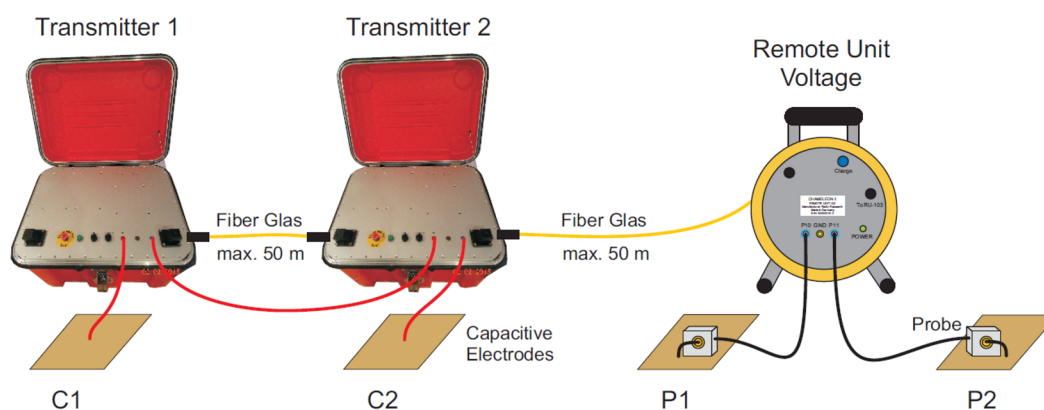
Figure 1. Arrangement of the components of the Chameleon II measuring system for capacitive and galvanic impedance measurements. The red lines are analog current cables. There is one transmitter at each current electrode. The remote unit, integrated in a cable drum, is connected to the potential electrodes via active probes and potential cables (black). Optic fibre cables (yellow) are used to avoid coupling effects. (Radic Research: Flyer Chameleon II)

15   ## 5   Field site and additional investigations

The Shestakovka River Basin in Central Yakutia, Russia, is a field site of the Melnikov Permafrost Insitute (Yakutsk). The area is located in the continuous permafrost zone. The field site and its geological features have been described by Lebedeva et al. (2019). The area is partially covered by pine forest and larch forest. Swamp-like zones occur along the creeks. Sandy

deposits dominate the top layers of the geological cross section. The thickness of permafrost in the area can be up to several hundred meters with an overlaying shallow active layer varying from $0.5\,\mathrm{m}$ to a maximum of $4\,\mathrm{m}$. The research of Lebedeva et al. (2019) focused on the occurrence of suprapermafrost subaerial talik and subsurface thermal anomalies that results in local unfrozen, water-bearing areas within the permafrost. The phenomenon is known to exist in Central Yakutia and in particular in

5   the area of Shestakovka River Basin. Their results from borehole analysis and geophysical measurements clearly indicate talik within the first few meters depth.

The location of the study area is presented in fig. 2. The ERT profile is an extension of the measurements from Lebedeva et al. (2019), named 'profile III'. In that context, the results of well 3/16-P were already discussed. That ERT profile was extended by $250\,\mathrm{m}$ in the north-east direction and now has a length of approximately $500\,\mathrm{m}$. On this profile extension, a new borehole was

10   drilled, named 'well 3/18'. The two-dimensional resistivity distribution from the ERT profile is displayed in fig. 3 south-west directed for the depth range up to $10\,\mathrm{m}$. While the right half of the profile was already part of the investigations in Lebedeva et al. (2019), the result of first half of the profile is presented for the first time. It also indicates on the profile extension (left half), albeit somewhat less pronounced, that areas of lower resistivity ($< 3000\,\Omega\mathrm{m}$) appear in the depth range above $10\,\mathrm{m}$. In these near-surface areas, thawed deposits within the permafrost, i.e. the talik areas, occur. Moreover, a high resistive zone

15   ($> 8000\,\Omega\mathrm{m}$) between profile meters 100 and 300 could indicate a higher ice content within the permafrost compared to the surrounding areas. The ERT results show that the talik is not a continuous layer, but is separated into water bearing channels orientated along the slope to the river (Lebedeva et al., 2019). Focusing on the subsurface structure of the first $10\,\mathrm{m}$ of depth, being the investigation area of the applied HFIP method, fig. 4 shows the results of the lithology, the soil moisture and the resistivity of the investigation from well 3/18. The subsoil consists of deposits of fine sand starting below a thin top-soil layer.

20   The thawed layer occurs between $2.2\,\mathrm{m}$ and $7.7\,\mathrm{m}$ depth, bounded above and below by permafrost. This structure is very similar to the borehole investigations from well 3/16-P, presented in Lebedeva et al. (2019). In order to obtain more accurate estimates of the thickness of the near-surface unfrozen layer, separate measurements during the time of the HFIP measurements were undertaken, showing a thickness slightly less than $50\,\mathrm{cm}$ along the HFIP profile. The soil moisture exhibits values up to around $20\,\%$ above the talik, increasing towards its upper boundary. The talik area itself is fully saturated. Since only frozen cores

25   were sampled from the borehole, data of the soil moisture are available only for the corresponding depth range. The resistivity in the borehole reaches values of around $5000\,\Omega\mathrm{m}$ at the surface, decreasing below $2000\,\Omega\mathrm{m}$ within the talik.

In May 2019, we performed a field survey with the HFIP method using the Chameleon-II device. Here, we focus on a line profile of $50\,\mathrm{m}$ extension, the position of which is also shown in fig. 2 (B to B$'$). The HFIP profile is defined south-west directed and starts around $40\,\mathrm{m}$ north-east of well 3/18. The measurements were carried out with a dipole-dipole configuration, with a

30   dipole length of $1.5\,\mathrm{m}$ and where the dipole spacing varied between $1.5\,\mathrm{m}$ and $42\,\mathrm{m}$. Overall, more than 100 impedance spectra were measured, with a frequency range from $2\,\mathrm{Hz}$ to $115\,\mathrm{kHz}$. Additionally a separate sounding in Schlumberger configuration with a maximum spacing of $\overline{AB} = 32\,\mathrm{m}$ was performed on the profile, at the location marked with C in fig. 3.
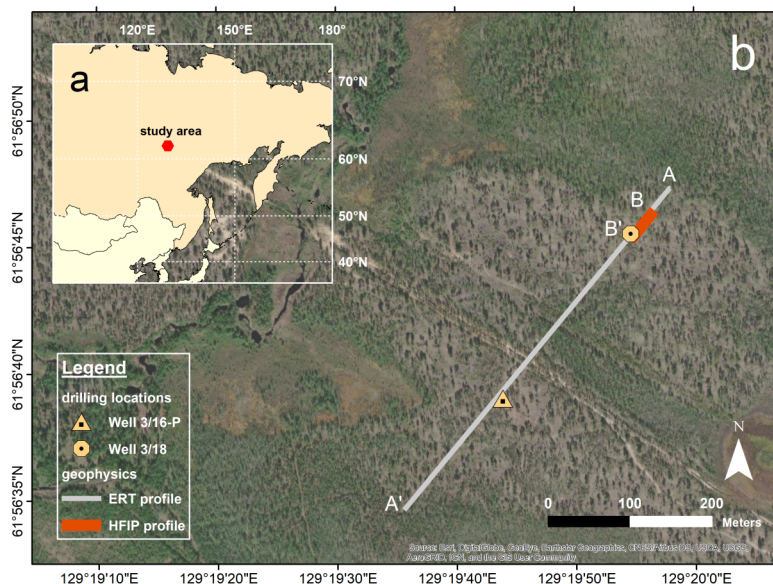
Figure 2. Geographical maps of the field site. Panel a gives an overview of the location of the study area in Russia. In Panel b the position of the ERT profile, directed from A to A′, and the HFIP profile from B to B′ are shown, as well as the locations of boreholes 3/16-P and 3/18.
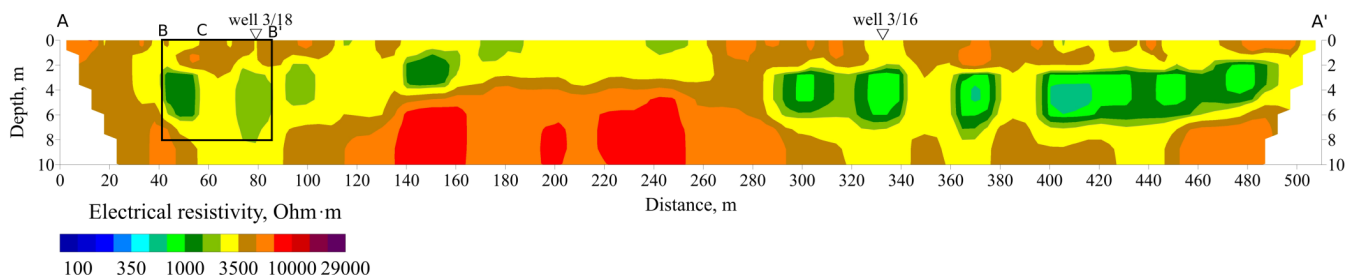
Figure 3. Two-dimensional section of the electrical resistivity over the whole ERT profile of around 500 m length (A to A′). The black rectangle marks the corresponding subsurface area of the HFIP measurements (B to B′), including the midpoint location of the HFIP sounding (C) and the location of well 3/18.

6   Results: the spectral signal of permafrost

A Schlumberger sounding was carried out with the midpoint location given in fig. 2. Since enlarging electrode distance corresponds with higher investigation depth (e.g. Militzer and Weber, 1985), the spectra should give a first overview of the depth distribution of permafrost. Since the method is still in its infancy, and only few case histories exist, we find it useful to discuss raw data and investigate the direct impact of the presence of ice in the measured spectra. The purpose is to illustrate how field data in a quasi-layered situation in a permafrost environment can look like and how the data varies with investigation depth.
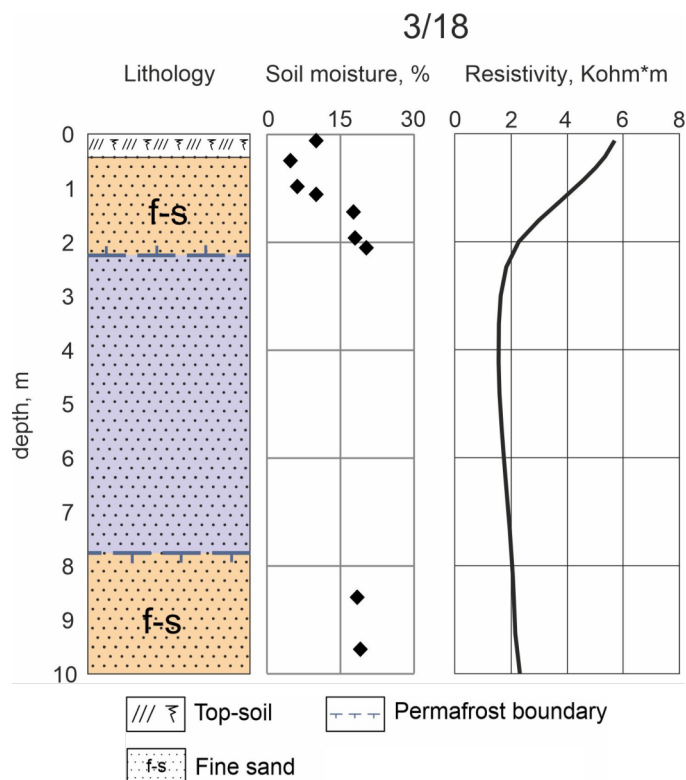
Figure 4. Cross section of well 3/18: the lithology, soil moisture and resistivity are displayed from left to right. The drilling and investigations are were conducted in April 2018. The blue area in the lithology section marks the unfrozen talik between the frozen areas displayed in yellow.

Two data sets, one for the smallest spacing ($\overline{AB} = 2\,\mathrm{m}$) and one for an intermediate spacing at $\overline{AB} = 12\,\mathrm{m}$, are shown in fig. 5. Every symbol corresponds to the magnitude and the phase shift of the impedance Z respectively for a discretely measured frequency. The phase shift is shown up to $115\,\mathrm{kHz}$, however, for the magnitude, values are only displayed until $60\,\mathrm{kHz}$, as the highest frequency values contain high errors. Note that the phase shift is just shown down to $-20°$, and not the full range for

5 the phase shift of $-90°$. The spectral signal of $\overline{AB} = 12\,\mathrm{m}$ shows a strong frequency dependence between $10^2 - 10^5\,\mathrm{Hz}$ with a clear peak, representing a single relaxation process. The data can be fitted by the Cole-Cole model (eq. 2), which provides the apparent parameters of the subsoil for every measured impedance spectra. The spectrum of the smallest spacing ($\overline{AB} = 2\,\mathrm{m}$) is distinctly different and does not show any clearly visible frequency dependence corresponding to the frequency behaviour of the ice relaxation process. The decreasing magnitude and phase shift for high frequencies is due to the overlap between

10 conduction and displacement current mechanism (see eq. 1). Fitting the data of the smallest spacing by the Cole-Cole model, the result for the relaxation time is around $10^{-2}\,\mathrm{s}$, much longer than expected for ice. Our interpretation is that the effect of ice is negligible or even not present for this electrode spacing, because of the unfrozen active layer at shallow depth. If we assume electrical parameters resistivity and permittivity as independent of frequency, the data can be fit by eq. 1. The resulting model
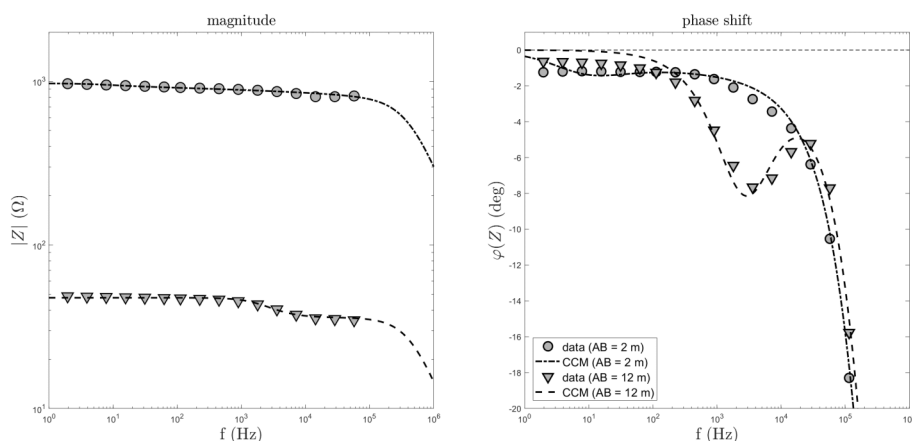
Figure 5. Spectra of the magnitude (left) and the phase shift (right) of the impedance Z for two measurements with electrode spacing $\overline{AB} = 2\,\mathrm{m}$ (dots) and $\overline{AB} = 12\,\mathrm{m}$ (triangles). The larger spacing, associated with higher investigation depth, shows a distinct frequency peak above $1\,\mathrm{kHz}$, whereas the other spacing shows weaker frequency dependence. The symbols indicate the measured data, the dashed lines are the data calculated for the single Cole-Cole model.

parameters are quite similar to the corresponding ones of the Cole-Cole model (tbl. 1). It is also possible to fit the data with a model for multiple relaxation processes. Tests with a Cole-Cole model of two relaxation terms (not shown here), resulted in a second relaxation for frequencies around $100\,\mathrm{Hz}$ and lower. This may fit the measured data for lower frequencies a little better, but leaves the high frequency relaxation nearly untouched. As we just focus on the high frequency mechanism, corresponding

5 to ice relaxation, we therefore take the single relaxation model as sufficient for our analysis.

The apparent Cole-Cole parameters obtained by the fitting process of all spacings are listed in table 1. Except for the smallest spacing, all model spectra show a relaxation process around $5 \times 10^{-5}\,\mathrm{s}$ which supports the assumption of ice relaxation. A closer look reveals systematic variations with increasing investigation depth. From the second smallest spacing on, both permittivity values are first increasing with depth and then decrease again towards largest spacing. The relaxation time varies

10 within a narrow range and decreases continuously with depth. The resistivity values increase for the first spacings and then decrease to the largest one. The model exponent c does not show consistent variation but its proximity to one supports the hypothesis of ice causing the relaxation, since it is known that ice relaxation can be described by the Debye model ($c = 1$) (e.g Petrenko and Whitworth, 2002). The quality of the fitting process for each data set is quantified by the root mean square (rms). The values are calculated as percentage rms for the magnitude spectra and absolute rms in radiant for the phase spectra.

15 The corresponding equations are presented for example by Przyklenk et al. (2016). All misfits are small, indicating that the Cole-Cole model is well suited to describe the measured spectra.

Table 1. Model parameters of the data fit for the different spacings of the sounding. The measured impedance spectra were fitted by the single Cole-Cole model (eq. 2) by five parameters. Additionally, for the smallest spacing another data fit with constant electrical parameters over frequency (eq. 1) was made. The data fit is quantified by the root mean squares.

spacing $\overline{AB}(m)$	$\rho_{DC}(\Omega m)$	ε_{DC}	ε_{HF}	$\tau(s)$	c	$rms_{|Z|}(\%)$	$rms_{\varphi}(mrad)$
2	$2.29 \cdot 10^3$	52441	21.6	$2.4 \cdot 10^{-2}$	0.84	0.29	6
	$2.13 \cdot 10^3$	–	21.2	–	–	0.57	13
4	$2.95 \cdot 10^3$	428	17.8	$7.0 \cdot 10^{-5}$	0.96	0.36	13
6	$3.15 \cdot 10^3$	492	17.5	$5.3 \cdot 10^{-5}$	0.98	0.41	13
8	$3.02 \cdot 10^3$	537	18.0	$5.2 \cdot 10^{-5}$	0.99	0.41	12
12	$2.61 \cdot 10^3$	705	19.4	$5.1 \cdot 10^{-5}$	0.99	0.47	11
16	$2.28 \cdot 10^3$	699	21.1	$5.1 \cdot 10^{-5}$	0.99	0.52	9
20	$2.18 \cdot 10^3$	607	21.4	$4.7 \cdot 10^{-5}$	0.99	0.62	9
26	$2.18 \cdot 10^3$	525	19.1	$4.2 \cdot 10^{-5}$	0.99	0.92	14
32	$2.14 \cdot 10^3$	512	16.2	$4.1 \cdot 10^{-5}$	1.00	0.97	12

Since the method is not yet well established, and the behaviour of the data in the presence and absence of ice is not generally known, we discuss the phase shift spectra in fig. 6. The left part corresponds to the spacings from $\overline{AB}$ 4 to 12 (fig 6a), the right one from $\overline{AB}$ 12 to 26 (fig 6b). All spectra show a characteristic peak with its minimum around a frequency of 10^4 Hz. However, for increasing investigation depth, the intensity of the relaxation, characterized by the minimum phase shift, rises up

5   gradually to $\overline{AB} = 12$ and further on decreases with higher investigation depth to $\overline{AB} = 26$. From the equation by Zorin and Ageev (2017) for a mixture of materials including ice it can be expected that as the ice content increases, so does the strength of the polarization, measured by the intensity of the peak in phase shifts. Modelling of pure ice, using the Debye relaxation (eq. 5) can result in a strong phase peak ($< -70°$) depending on the model parameters, in particular on the resistivity. Such strong phase peaks were indeed observed during by field measurements (unpublished) with the Chameleon II device on alpine

10   glacier ice, where values for the phase peak down to $-80°$ were measured. For a typical two-layer case of permafrost, with an unfrozen active layer above the frozen layer, measurements should show an increasing phase peak with investigation depth. This expected behaviour agrees well with calculated data in fig. 6a. The reduction of the phase peak for even greater spacing indicates a decrease of ice content with depth (fig. 6b). This suggests either a significant decrease of ice content in the deeper permafrost areas or even an unfrozen layer. Our a priori knowledge about the existence of talik in the permafrost layer at the

15   field site from the ERT and borehole investigations (fig. 3 & 4), points at an unfrozen layer as the most likely explanation.
One potential uncertainty of interpreting the occurrence of subsurface ice based on DC resistivity information only, is its ambiguity. Different materials and moreover different compositions can fall into in the same range of resistivity values. Thus, for an interpretation of the subsurface, in particular with respect to ice occurrence, additional information is indispensable. In case of our results (tbl. 1), the resistivity exhibits variations with respect to investigation depth, but its range is rather

20   limited. A categorization just based on the results of resistivity measurements seems difficult. In contrast, the spectral signal of ice provides an almost unambiguous footprint. Thus we have an indicator whether ice is present or not, within the sensitive
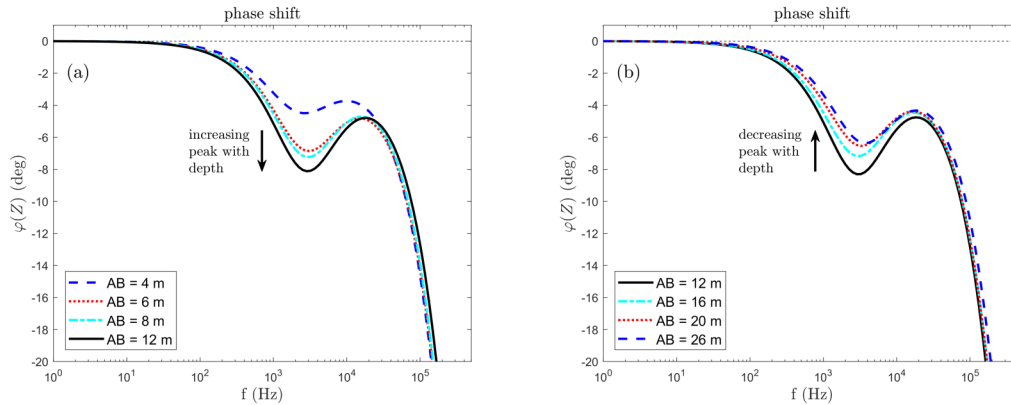
Figure 6. Calculated phase shift spectra for the Cole-Cole models used to fit the Schlumberger sounding data for the spacings $\overline{AB} = 4 - 12\,\text{m}$ (left) and for $\overline{AB} = 12 - 26\,\text{m}$ (right). The model fit of the data $\overline{AB} = 12\,\text{m}$ (black curve) is shown in both panels. All curves show a strong frequency dependence between $10^2 - 10^5\,\text{Hz}$, whereby the intensity of phase peak gradually increases up to the spacing $\overline{AB} = 12\,\text{m}$ and decreases again for larger spacings.

volume, if the full spectral signal is measured.

7   Results: Ice Content Estimation

A spectral 2-D inversion was carried out using the inversion tool AarhusInv (Auken et al., 2014). The procedure provides a
5   spatial distribution of the five Cole-Cole parameters defined by eq. 2, and the result is shown in fig. 7. Brighter areas in the lower parts of each section are those regions where the maximum depth for reliable parameter estimation based on the depth-of-investigation estimate by (Fiandaca et al., 2015) is exceeded. The full spectral inversion algorithm calculates the distribution of the model parameters simultaneously over all frequencies and electrode configurations. The misfit of the inversion is calculated by the weighted mean square error over all inverted spectra, denoted by the symbol χ (Fiandaca et al., 2013). For the result
10   shown in fig. 7, the misfit is $\chi = 1.9$.

The resistivity (panel a) is the same as determined by other electric or electromagnetic methods, for example by ERT, and can be compared with those results. The image is characterized by a high resistive layer above a depth of $2\,\text{m}$. Underneath, two areas of low resistivity occur, where the one on the left half of the profile has a larger extension than the one on the right half. The areas are interpreted as water-bearing, unfrozen talik, according to (Lebedeva et al., 2019). The two talik zones are embedded
15   in a background resistivity of around $3000\,\Omega\text{m}$ and seem to be separated around profile coordinate $25\,\text{m}$. Directly under the surface, a very shallow layer of lower resistivities is present, which may indicate a thin unfrozen active layer. Separately performed direct measurements of the unfrozen surface area during the days of geophysical measurements revealed an active layer thickness in the range of $30 - 50\,\text{cm}$ along the profile.

The other model parameters in fig. 7 show significant spatial variation as well, although the supposed talik areas are not as clearly visible as for the resistivity. The values for the model exponent c (panel e) are close to 1, and only deviate for the supposedly unfrozen areas of talik and within the first meter. This is consistent with the fact that the Debye relaxation model ($c = 1$) describes the frequency dependence of ice, and $c = 1$ could therefore be an indicator for the location of frozen ground.

5   The low frequency permittivity (panel b) and the relaxation time (panel d) exhibit a layered structure, with a distinct layer in about $1 - 3\,\mathrm{m}$ depth. The relaxation time for this layer is in the range of literature value for ice relaxation close to the melting point. Above, the times increases, which means that relaxation process is shifting towards lower frequency ranges. The high frequency permittivity (panel c) has higher values within the first meter in depth and at an anomaly at the end of the profile. Below $1\,\mathrm{m}$, ε_{HF} jumps to significantly smaller values. As the high-frequency permittivity of ice is characteristically low ($3-4$),

10   areas of low values may indicate significant ice content.

The result for the DC resistivity parameter (panel a) is in good agreement with the corresponding ERT 2-D result, which is displayed in fig. 8. The two separated low resistive areas are present in both images, as well as the high resistive layer above. The boundary between those layers is consistent with the results obtained in well-3/18 (fig. 4), indicating the transition from permafrost to the unfrozen area in $2.2\,\mathrm{m}$ depth at the borehole location. The shallow surface layer is only visible in the

15   resistivity result of the HFIP due to the higher resolution compared to the large ERT profile.

The results and the interpretation as areas of talik embedded in the permafrost with a shallow active layer, is supported by the data of the Schlumberger sounding as well. The Schlumberger sounding is able to identify the basic structure of the talik embedded in permafrost, but of course, in order to reveal the variation along the profile, including the separation of the two talik structures, a 2-D data acquisition and inversion is required.

20   Within a next step, we transfer the frequency dependent information of the Cole-Cole model distribution into a value of ice content. For this purpose, the two-component model (eq. 3) after Zorin and Ageev (2017) was applied to the results of the 2-D inversion. For every cell of the inversion grid, the ice content is determined using the procedure described in chapter 3 and the result is presented in fig. 9. Overall, the distribution of ice content gives a coherent picture, consistent with the expectations: Near the surface, a distinct layer with non-zero ice content between approx. $1\,\mathrm{m}$ and $2.5\,\mathrm{m}$ depth is embedded between layers

25   of zero or almost zero ice-content. At greater depths below $6\,\mathrm{m}$, the ice content increases again. The near-surface layer with zero ice-content corresponds to the currently unfrozen part of the active layer. The distinct layer with highest ice content is the frozen part of the soil with significant moisture, whereas the zones with zero ice content between $3\,\mathrm{m}$ and $7\,\mathrm{m}$ depth correspond to the unfrozen talik.

The borehole information on frozen and unfrozen state, in combination with the soil moisture measurements (fig. 4) even

30   allows a quantitative assessment of the estimated ice content. The soil moisture in the frozen sections of the borehole can be directly transferred to ice content. Just above the talik, in approx. $2.2\,\mathrm{m}$ m depth, the soil moisture, and thus the ice content, reaches values of approx. $20\,\%$ with an increasing tendency with depth. Close to the boundary to the talik, the ice content may be expected to be almost as high as in the unfrozen talik itself. The water content within the talik was not measured for well 3/18, but investigations by (Lebedeva et al., 2019) indicate contents of $30\,\%$ and more. Therefore, it can be expected that the
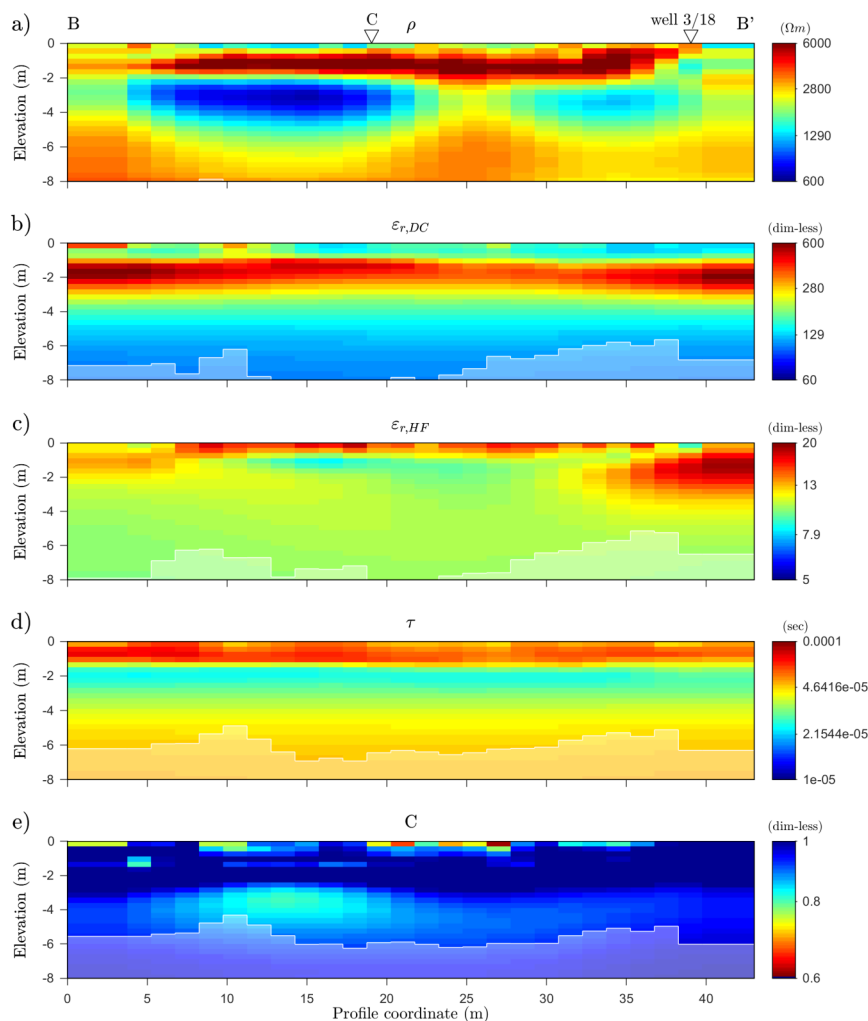
Figure 7. Two-dimensional inversion results for the profile of HFIP measurements at the Shestakovka River basin (B to B′), separately shown for each of the five Cole-Cole parameters (a-e). The total data fit is $\chi = 1.9$. Brighter areas mark zones of decreased reliability based on the depth of investigation (Fiandaca et al., 2015). The locations of the Schlumberger sounding (C) and the well 3/18 are marked additionally at panel a.

ice content just above the talik can reach values larger than 20%, or even up to 30%. The values of the HFIP-estimated ice content at the location of well 3/18 (fig. 9) are in the range of 25%, which is consistent with the borehole-derived estimates within approx. 5%. Away from the borehole, ice content values up to 35% are reached with can also be considered realistic. The lower boundary of the talik at the location of well 3/18 is approx. at $7.7\,\mathrm{m}$ depth (fig. 4). In the HFIP results (fig. 9), the ice content at the location of well 3/18 increases to values above zero in slightly shallower depths, around $6\,\mathrm{m}$. However, temperature measurements in well 3/18 indicate that the boundary to the frozen zone ($< 0.1\,°\mathrm{C}$) actually moves and can vary
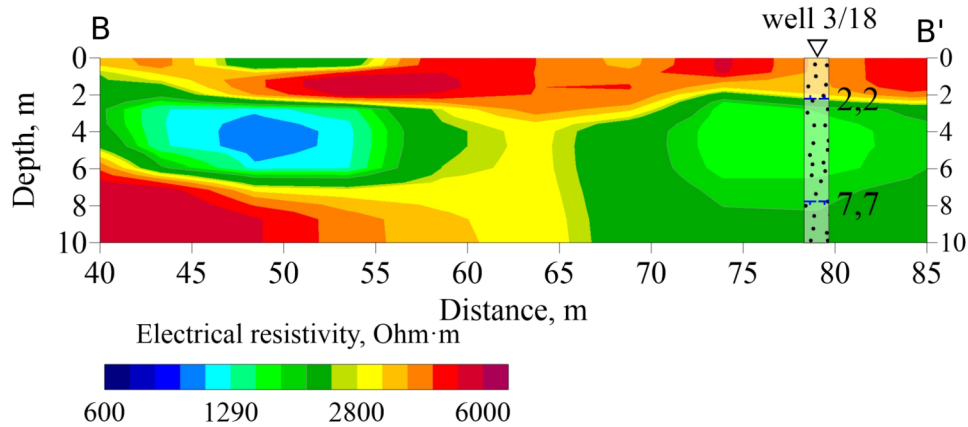
Figure 8. Two-dimensional electrical resistivity as results of the ERT inversion. Displayed is the part from profilemeter 40 to 85 of the bigger section in fig. 3 that corresponds to the section of the HFIP inversion in fig. 7 (B to B$'$). Additionally, the location of well 3/18 and its estimated boundaries from permafrost to the unfrozen layer are shown.
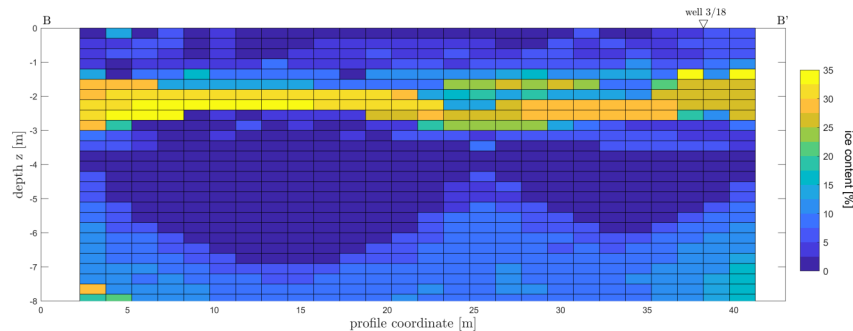
Figure 9. Ice Content α in percent over the two-dimensional profile, calculated using the procedure describe in chapter 3. The displayed section is the same as in fig. 7 (B to B$'$).

between $5\,\mathrm{m}$ and $9\,\mathrm{m}$. If we also consider that the inversion algorithm uses a regularization and there is a natural limit to the accuracy at which the depth of boundaries can be determined, the HFIP result can be considered consistent with the borehole information. Quantitatively, the HFIP estimated ice content does not quite reach the values around $17\,\%$ indicated by the soil moisture, which can also be attributed to the regularization and the decreasing spatial coverage at greater depths.

5 To evaluate the feasibility of the ice content estimation model, we use the data fit resulting from fitting eq. 3 to the Cole-Cole model obtained from the inversion. For each inversion cell, the misfit is expressed in terms of root mean square (rms) values and displayed for magnitude and phase shift spectra in fig. 10, in the same fashion as the ice content itself. Except for a few outliers, the rms values are below $20\,\%$ for the magnitude and below $0.15\,\mathrm{rad}$ for the phase shift. For depth ranges lower than $1\,\mathrm{m}$ and greater than $2.5\,\mathrm{m}$, the data exhibits small fitting errors. In contrast, for the area in between, both rms panels show

10 higher values. This area represents the layer of significantly higher ice content above the talik. The increasing fitting errors for
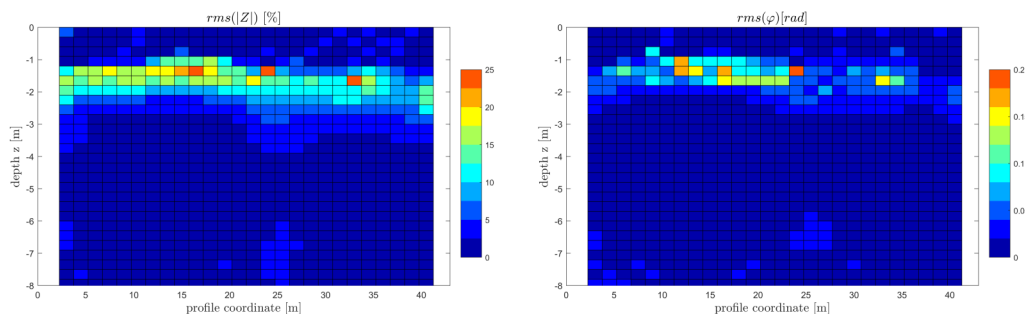
Figure 10. Data fit of the ice content estimation in terms of the root mean square for the magnitude $|Z|$ (left panel) and the phase shift φ (right panel). The values are displayed for every inversion cell over the 2-D profile.

large ice content indicate that eq. 3 might no longer match perfectly with the Cole-Cole model, and that further improvements might be achieved by modifications of the ice content model.

8   Conclusions

Broad-band observations of complex electrical resistivity were carried out on a permafrost field site close to the Sibirian
5   city Yakutsk. We used the novel complex resistivity measurement device "Chameleon-II", designed for studying electrical dispersion in a wide frequency range in highly resistive regions, especially under cryospheric conditions. The data analysis is performed by fitting a permittivity Cole-Cole model to the measured spectra, either for single measurements or within a 2-D inversion, to extract the strong frequency dependent behaviour of ice dispersion. Based on the Cole-Cole inversion, we implemented a 2-D estimation of the subsurface ice content using an existing two-component complex resistivity model of
10   frozen soil.

The evaluation of the measured HFIP spectra shows a characteristic dispersion in the expected frequency range is caused by the known electrical dispersion of ice. A systematic variation of the spectra with the investigation depth is observed, which is reasonably consistent with the structure and measured values from previous borehole and ERT investigations. The unfrozen area within the permafrost body, as well as the shallow active layer, can be distinguished from the areas of frozen ground.

15   We conclude that the HFIP method in combination with our novel procedure to estimate ice content is a useful tool for permafrost research at the field scale. The method is able to separate frozen from unfrozen ground, and more importantly, to provide quantitative estimates of ice content. In the case study discussed here, the estimated ice content values were close to zero where the ground is unfrozen, and larger than zero in frozen sections. Quantitatively, the estimated values were fairly consistent with ice contents determined from soil moisture data obtained from borehole samples. Our results indicate that the
20   relationships between ice content and electrical properties obtained by theoretical considerations and in the laboratory, can actually have a practical value at the field scale.

At the local scale, our study confirms the supposed existence of taliks along the profile by verifying that the low resistive zones

along the profile indeed have zero ice content. We also conclude that the Chameleon II equipment with its specific electronic concept to avoid EM coupling is feasible and sufficiently robust to be applied over highly resistive ground typically encountered in permafrost research.

The new approach to estimate ground ice content at the field scale using full spectral information, encourages future research.

5 First, it might be conceivable to combine our method and its advantages with existing models, such as the ice content inversion by Wagner et al. (2019) based on the model from Hauck et al. (2011), to further reduce ambiguity inherent in each separate method. Second, the method might be advanced to explore even greater depths. Currently, we are limited by the maximum distance between transmitter and receiver of $50\,\mathrm{m}$, which was considered a maximum reasonable length where distortions by EM coupling could be sufficiently reduced by the specific measuring electronics. The encouraging results obtained here

10 indicate that it could be worthwhile to put further efforts into the development of the measuring system. In that context, EM induction effects that cannot be avoided by measuring technology, will also play a greater role. These effects increase with the square of the spatial scale, which might require correction or simulation procedures, if greater depths will be investigated.

The relationship between ice content and the parameters that can actually be extracted from the field data will also require further attention. Here, we build on the two component model Zorin and Ageev (2017), but the increasing fitting error with

15 increasing ice content observed in our case study might indicate that further improvements could be achieved by modifications of the model.

Code and data availability.   The HFIP data measured at the field site are available on request to Jan Mudler (j.mudler@tu-bs.be). Access to AarhusInv software can be requested at https://hgg.au.dk/software/aarhusinv/.

Author contributions.   JM, KB and LL performed the different measurements in the field and analyzed the data. DK and JM developed the
20 code for the ice content estimation. AH supported the whole process of research and wrote several sections of the article. TR developed and built the measurement device and its software. JM prepared the manuscript with contribution from all co-authors.

Competing interests.   The authors declare that they have no conflict of interest.

Acknowledgements.   We are greatful to Malte Lührs (TU Braunschweig) for his support of our measurements in Yakutia and Madhuri Sugand and Johannes Buckel (both TU Braunschweig) for proofreading and support on the manuscript.
25 The work was sponsored by the German Research Foundation DFG (project HO 1506/22-2). The reported study was partially funded by the Russian Foundation for Basic Research RFBR (projects 20-35-70027 and 20-05-00670).

References

Artemov, V.: A unified mechanism for ice and water electrical conductivity from direct current to terahertz, Phys Chem Chem Phys, 21, 8067 – 8072, https://doi.org/10.1039/c9cp00257j, 2019.

Artemov, V. and Volkov, A.: Water and Ice Dielectric Spectra Scaling at 0 °C, Ferroelectrics, 466, 158 – 165, https://doi.org/10.1080/00150193.2014.895216, 2014.

Auken, E., Christiansen, A., Kirkegaard, C., Fiandaca, G., Schamper, C., Behroozmand, A., Binley, A., Nielsen, E., Effersø, F., Christensen, N., Sørensen, K., Foged, N., and Vignoli, G.: An overview of a highly versatile forward and stable inverse algorithm for airborne, ground-based and borehole electromagnetic and electric data, Explor Geophys, 46, 223 – 235, 2014.

Auty, R. and Cole, R.: Dielectric Properties of Ice and Solid D2O, J Chem Phys, 20, 1309 – 1314, https://doi.org/https://doi.org/10.1063/1.1700726, 1952.

Bittelli, M., Flury, M., and Roth, K.: Use of dielectric spectroscopy to estimate ice content in frozen porous media, Water Resour Res, 40, W04 212, https://doi.org/doi:10.1029/2003WR002343, 2004.

Cole, K. and Cole, R.: Dispersion and Absorption in Dielectrics: 1.Alternating Current Characteristics, J Chem Phys, 9, 341 – 351, 1941.

Fiandaca, G., Ramm, J., Binley, A., Gazoty, A., Christiansen, A., and Auken, E.: Resolving spectral information from time domain induced polarization data through 2-D inversion, Geophys J Int, 192, 631 – 646, 2013.

Fiandaca, G., Christiansen, A., and Auken, E.: Depth of Investigation for Multi-parameters Inversions, European Association of Geoscientists and Engineers. Near Surface Geoscience 2015. Conference Paper, 631 - 646, 2015.

Grimm, R. and Stillman, D.: Field Test of Detection and Characterisation of Subsurface Ice using Broadband Spectral-Induced Polarisation, Permafrost Periglac, 26, 28 – 38, 2015.

Grimm, R., Stillman, D., and MacGregor, J.: Dielectric signatures and evolution of glacier ice, J Glaciol, 61, 1159 – 1170, 2015.

Hauck, C. and Kneisel, C.: Applied Geophysics in Periglacial Environments, Cambridge Univ. Press, 2008.

Hauck, C., Böttcher, M., and Maurer, H.: A new model for estimating subsurface ice content based on combined electrical and seismic data sets, Cryosphere, 5, 453 – 468, 2011.

Heginbottom, J., Brown, J., Humlum, O., and Sennson, H.: Permafrost and periglacial environments, In State of the Earth's Cryosphere at the Beginning of the 21st Century, Williams R, Ferrigno J (eds), USGS Professional Paper 1386-A-5, p. 546, 2012.

Hippel, A.: The Dielectric Relaxation Spectra of Water, Ice and Aqueous Solutions, and their Interpretation, IEEE T Electr Insul, 23, No. 5, 801 – 816, https://doi.org/doi:10.1109/14.8744, 1988.

Kemna, A., Binley, A., Ramirez, A., and William, D.: Complex resistivity tomography for environmental applications, Chem Eng J, 77, 11 – 18, 2000.

Kozhevnikov, N. and Antonov, E.: Fast-decaying inductively induced polarization in frozen ground: A synthesis of results and models, J Appl Geophys, 82, 171 – 183, https://doi.org/10.1016/j.jappgeo.2012.03.008, 2012.

Lebedeva, L., Bazhin, K., Khristoforov, I., Abramov, A., Pavlova, N., Efremov, V., Ogonerov, V., Tarbeeva, A., Fedorov, M., Nesterova, N., and Makarieva, O.: Suprapermafrost subaerial taliks, Central Yakutia, Shestakovka River Basin, Earth's Cryosphere, 23, 35 – 4, 2019.

Limbrock, J. and Weigand, M.: Improved thermal characterization of alpine permafrost sites by broadband SIP measurements, Conference: EGU General Assembly 2020, https://doi.org/10.5194/egusphere-egu2020-20081, 2020.

Loewer, M., Günther, T., Igel, J., Kruschwitz, S., Martin, T., and Wagner, N.: Ultra-broadband electrical spectroscopy of soils and sediments - a combined permittivity and conductivity model, Geophys J Int, 210, 1360 – 1373, 2017.

Militzer, H. and Weber, F.: Angewandte Geophysik,2 :Geoelektrik-Geothermik-Radiometrie-Aerogeophysik, Springer Wien, Akademie-Verlag Berlin, 1985.

Mollaret, C., Wagner, F., Hilbich, C., Scapozza, C., and Hauck, C.: Petrophysical Joint Inversion Applied to Alpine Permafrost Field Sites to Image Subsurface Ice, Water, Air, and Rock Contents, Front Earth Sci, 8, id 85, https://doi.org/https://doi.org/10.3389/feart.2020.00085, 2020.

Mudler, J., Hördt, A., Przyklenk, A., Fiandaca, G., Maurya, P., and Hauck, C.: Two-dimensional inversion of wideband spectral data from the capacitively coupled resistivity method - first applications in periglacial environments, Cryosphere, 13, 2439 – 2456, https://doi.org/https://doi.org/10.5194/tc-13-2439-2019, 2019.

Petrenko, V. and Whitworth, R.: Physics of Ice, Oxford University Press, New York, 2002.

Przyklenk, A., Hördt, A., and Radić, T.: Capacitively-Coupled Resistivity measurements to determine frequency-dependent electrical parameters in periglacial environments - theoretical considerations and first field tests, Geophys J Int, 206, 1352 – 1365, 2016.

Radić, T.: First Results from the New Multi-purpose Instrument CapGeo, 19th European Meeting of Environmental and Engeneering Geophysics, Near Surface Geoscience, TuP15, https://doi.org/doi:10.3997/2214-4609.20131364, 2013.

Sasaki, K., Kita, R., Shinyashiki, N., and Yagihara, S.: Dielectric Relaxation Time of Ice-Ih with Different Preparation, J Phys Chem B, 120, 3950 – 3953, https://doi.org/https://doi.org/10.1021/acs.jpcb.6b01218, 2016.

Schuur, E., McGuire, A., Schädel, C., Grosse, G., Harden, J., Hayes, D., Hugelius, G., Koven, C., Kuhry, P., Lawrence, D., Natali, S., Olefeldt, D., Romanovsky, V., Schaefer, K., Turetsky, M., Treat, C., and Vonk, J.: Climate change and the permafrost carbon feedback, Nature, 520, 171 – 179, https://doi.org/doi:10.1038/nature14338, 2015.

Stillman, D. and Grimm, R.: Low-Frequency Electrical Properties of Ice-Silicate Mixtures Regoliths, J Phys Chem-US, 114, 6065 – 6073, 2010.

Wagner, F., Mollaret, C., Günther, T., Kemna, A., and Hauck, C.: Quantitative imaging of water, ice and air in permafrost systems through petrophysical joint inversion of seismic refraction and electrical resistivity data, Geophys J Int, 219, Issue 3, 1866 – 1875, https://doi.org/10.1093/gji/ggz402, 2019.

Weidelt, P.: Grundlagen der Geoelektrik, in Handbuch zur Erkundung des Untergrundes von Deponien und Altlasten, pp. 65-94, ed. Knödel, K., Krummel, H., Lange, G., Band 3: Geophysik, Springer, Berlin, 1997.

Zorin, N. and Ageev, D.: Electrical properties of two-component mixtures and their application to high-frequency IP exploration of permafrost, Near Surf Geophys, 15, 603 – 613, 2017.